AGU PUBLICATIONS

JGR

Journal of Geophysical Research: Atmospheres

RESEARCH ARTICLE
10.1002/2014JD022576

Key Points:
- The origins of subdecadal GMT variability are consistent among GCMs
- The origins of interdecadal GMT variability are inconsistent among GCMs
- GCMs with interdecadal GMT variability from Southern Ocean have more variable GMT

Supporting Information:
- Readme
- Text S1 and Figures S1–S14

Correspondence to:
P. T. Brown,
Patrick.Brown@duke.edu

Citation:
Brown, P. T., W. Li, and S.-P. Xie (2015), Regions of significant influence on unforced global mean surface air temperature variability in climate models, *J. Geophys. Res. Atmos.*, *120*, doi:10.1002/2014JD022576.

Received 12 SEP 2014
Accepted 21 DEC 2014
Accepted article online 9 JAN 2015

Regions of significant influence on unforced global mean surface air temperature variability in climate models

Patrick T. Brown[1], Wenhong Li[1], and Shang-Ping Xie[2]

[1]Earth and Ocean Sciences, Nicholas School of the Environment, Duke University, Durham, North Carolina, USA, [2]Scripps Institution of Oceanography, University of California, San Diego, La Jolla, California, USA

Abstract We document the geographic regions where local variability is most associated with unforced global mean surface air temperature (GMT) variability in Coupled Model Intercomparison Project Phase 5 coupled global climate models (GCMs) at both the subdecadal and interdecadal timescales. For this purpose, *Regions of Significant Influence* on GMT are defined as locations that have a statistically significant correlation between local surface air temperature (SAT) and GMT (with a regression slope greater than 1), and where local SAT variation leads GMT variation in time. In both GCMs and observations, subdecadal timescale GMT variability is most associated with SAT variation over the eastern equatorial Pacific. At the interdecadal timescale, GMT variability is also linked with SAT variation over the Pacific in many GCMs, but the particular spatial patterns are GCM dependent, and several GCMs indicate a primary association between GMT and SAT over the Southern Ocean. We find that it is difficult to validate GCM behavior at the interdecadal timescale because the pattern derived from observations is highly depended on the method used to remove the forced variability from the record. The magnitude of observed GMT variability is near the ensemble median at the subdecadal timescale but well above the median at the interdecadal timescale. GCMs with a stronger subdecadal relationship between GMT and SAT over the Pacific tend to have more variable subdecadal GMT while GCMs with a stronger interdecadal relationship between GMT and SAT over parts of the Southern Ocean tend to have more variable GMT.

1. Introduction

Global mean surface air temperature (GMT) is one of the most recognized metrics of climate change on a range of timescales. Therefore, variability in GMT is of great interest to the scientific community as well as to the general public. Changes in GMT can result both from external radiative forcings [*Bindoff et al.,* 2013] and from internally generated unforced variability [*Hasselmann*, 1976; *Hawkins and Sutton*, 2009; *Leith*, 1978]. External radiative forcings change GMT by imposing an energy imbalance at the top of the atmosphere and include both anthropogenic (e.g., changes in greenhouse gas concentration, aerosols, and land use) and natural (e.g., changes in solar radiation and volcanic aerosols) influences. Unforced variability in GMT emerges out of the internal dynamics of the ocean-atmosphere system, involving a vertical redistribution of heat within the climate system (e.g., the movement of heat between the ocean and the atmosphere) [*Meehl et al.,* 2013; *Trenberth et al.,* 2002] and/or a change in the Earth's top-of-atmosphere energy budget which effects the total amount of heat in the system [*Brown et al.,* 2014; *Palmer and McNeall*, 2014].

It is well established that the observed centennial-scale warming of GMT since the industrial revolution has been primarily caused by external forcings and increased greenhouse gas concentrations in particular [*Bindoff et al.,* 2013]. Equally well established is that nonseasonal variability in GMT, on subdecadal timescales, tends to be dominated by unforced variability [*Brown et al.,* 2012; *Easterling and Wehner*, 2009; *Hawkins and Sutton*, 2009]. The primary exception to this is the response to a major volcanic eruption. At the interdecadal timescale (variability with characteristic timescales from ~10 to ~100 years), however, the magnitude of unforced GMT variability is still uncertain. This is exemplified in the ongoing debate concerning the relative importance of forced versus unforced influences on interdecadal variability in the rate of warming over the twentieth century (i.e., strong warming from the 1910s to 1940s, steady temperatures until the 1970s, strong warming until the late 1990s). Several studies have argued that this variability (superimposed on top of long-term forced warming) was a result of corresponding variability in external radiative forcings

[*Hansen et al.,* 2005; *Stott et al.,* 2006, 2000; *Wilcox et al.,* 2013; *Wild*, 2009]. Alternatively, these fluctuations may have been caused by changes in sign of unforced modes of variability internal to the climate system [*Chylek et al.,* 2014; *Crowley et al.,* 2014; *England et al.,* 2014; *Meehl and Teng*, 2014; *Swanson and Tsonis*, 2009; *Tung and Zhou*, 2013; *Wu et al.,* 2011].

Even within the literature that attributes twentieth century interdecadal GMT variation to unforced variability, there is substantial disagreement on what modes of variability (and thus geographic regions) are most associated with GMT changes. The two regions that are most often evoked as being particularly influential on interdecadal GMT variability are the North Atlantic Ocean and the Pacific Ocean. The North Atlantic is typically thought to influence GMT via the Atlantic Multidecadal Oscillation (AMO) [*Kerr*, 2000], and the Pacific Ocean is usually thought to influence GMT via low-frequency variability in the El Niño–Southern Oscillation (ENSO) [*Vimont*, 2005; *Zhang et al.,* 1997], the Interdecadal Pacific Oscillation (IPO) [*Power et al.,* 1999], or the Pacific Decadal Oscillation (PDO) [*Mantua et al.,* 1997]. Most studies do not agree on the relative influence of these regions on GMT and tend to emphasize either the North Atlantic's influence [*Chen and Tung*, 2014; *Chylek et al.,* 2014; *DelSole et al.,* 2010; *Delworth and Knutson*, 2000; *Hunt*, 2011; *Keenlyside et al.,* 2008; *Kravtsov and Spannagle*, 2008; *McGregor et al.,* 2014; *Muller et al.,* 2013; *Schlesinger and Ramankutty*, 1994; *Semenov et al.,* 2010; *Swanson et al.,* 2009; *Tung and Zhou*, 2013; *Wu et al.,* 2011; *Wyatt and Curry*, 2013; *Zhang et al.,* 2007] or the Pacific's influence [*England et al.,* 2014; *Huber and Knutti*, 2014; *Kosaka and Xie*, 2013; *Meehl et al.,* 2013; *Meehl and Teng*, 2014; *Risbey et al.,* 2014; *Trenberth and Fasullo*, 2013].

Understanding GMT variability and the internal modes that contribute most to this variability is critical for understanding past and predicting future climate change. In particular, the attribution of GMT change to external forcings requires coupled global climate models (GCMs) with accurate representations of baseline internal variability for the purpose of statistical hypothesis testing. Furthermore, the emerging field of "decadal prediction" [*Meehl et al.,* 2009; *Smith et al.,* 2007] requires that GCMs correctly simulate the processes and modes of variability that contribute most to GMT change on interannual to decadal timescales. With these issues in mind, the present work seeks to shed light on the following questions:

1. Do current GCMs act in accordance with the established finding that the eastern equatorial Pacific has the largest influence on unforced GMT variability on subdecadal timescales? Do GCMs accurately simulate the magnitude of unforced subdecadal GMT variability?
2. Do GCMs lend more support to the notion that interdecadal variability in GMT is associated with surface air temperature (SAT) variability in the North Atlantic or the Pacific? (SAT and sea surface temperature anomalies are highly correlated at these timescales.) Are there other locations that influence interdecadal GMT variability in some GCMs? Do GCMs accurately simulate the magnitude of interdecadal GMT variability?
3. What are the first-order physical processes that contribute to GMT variability in GCMs and is there any relationship between the magnitude of simulated GMT variability and the underlying modes associated with that variability?

The remainder of the paper is structured as follows: Section 2 gives the background and justification of a methodology (Regions of Significant Influence (ROSI)) that seeks to identify the locations that are most influential on unforced GMT variability. Section 3 discusses the observational and GCM data that the ROSI methodology is applied to. Section 4 presents the key results of the ROSI methodology, applied at both the subdecadal and interdecadal timescales. Section 5 discusses the primary findings inferred across the multimodel ensemble with an emphasis on first-order physical processes that may be responsible for the GCM-simulated variability. This section also analyzes the relationship between the underlying modes associated with GMT variability and the magnitude of simulated GMT variability across the model suite. Finally, a summary is presented in section 6.

2. Regions of Significant Influence on GMT in Observations and GCMs

Changes in GMT do not typically result from globally coherent variations in SAT. For example, it is well known that dynamics associated with the El Niño–Southern Oscillation (ENSO) can affect GMT [*Foster and Rahmstorf*, 2011; *Privalsky and Jensen*, 1995; *Trenberth et al.,* 2002; *Wigley*, 2000], but this effect is heavily influenced by SAT anomalies in the central/eastern equatorial Pacific rather than emerging from a coherent, globally uniform change in SAT [*Deser et al.,* 2010; *Messié and Chavez*, 2011; *Trenberth et al.,* 2002]. Therefore, it is reasonable to expect that SAT variation (and by proxy, modes of variability) will be more or less associated with GMT change depending on the region.

In order to quantify the influence of various modes of variability on GMT, predefined climatic indices are sometimes compared to GMT via regression/correlation analysis. For example, *Muller et al.* [2013] performed cross-correlation analysis between various climate indices and land GMT, while others have used ENSO indices or the AMO as predictors of GMT in multiple linear regression analysis [*Chylek et al.,* 2014; *Foster and Rahmstorf*, 2011; *Zhou and Tung*, 2012]. Such methodology can be problematic if the climate index does not fully capture the underlying physical mode's influence on GMT. For example, the AMO is sometimes defined as the detrended, basin mean, sea surface temperature of the Atlantic from 0°N to 60°N [*Enfield et al.,* 2001]. However, temperatures do not necessarily vary coherently within this domain [*Delworth et al.,* 2007; *Deser et al.,* 2010; *Zhang and Wang*, 2013]. If only part of this domain has a strong association with GMT, then the act of averaging over the entire domain will obscure this relationship. This is especially true in the case of the IPO and PDO indices which have positive and negative temperature anomalies incorporated into their characteristic pattern [*Mantua et al.,* 1997; *Power et al.,* 1999]. Furthermore, an underlying physical mode may work to influence GMT through complex teleconnections and feedbacks that may not be represented by a given index.

To avoid the aforementioned difficulties, we refrain from using a priori defined climatic indices to represent modes of variability. Instead, we allow each GCM to present the global SAT patterns most associated with its unforced GMT variability. This general strategy has been successful at identifying the IPO as a primary mode responsible for interdecadal GMT variability in at least one GCM [*Meehl et al.,* 2011, 2013], but here we extend this strategy to 34 GCMs. In our methodology, we regress local SAT at each global grid location against GMT in each of the GCM's unforced control runs, at both the subdecadal and interdecadal timescales. Additionally, we define *Regions of Significant Influence* (ROSIs) on GMT, which are grid points that, at a given timescale, had the following characteristics:

1. Local SAT and GMT had a statistically significant correlation (at 95% confidence level) at zero time lag, suggesting high coherence between a physical climatic mode at the given location and GMT. Statistical significance was calculated with a Monte Carlo method that accounted for persistence in the time series data (see supporting information).
2. Local SAT change preceded GMT changes, suggesting that local dynamics were primarily influencing, rather than responding to, changes in the global climate. The lead-lag relationship was obtained by identifying the time lag with the highest cross-correlation value between the local SAT time series and the GMT time series with a maximum lag of ±6 months for the subdecadal timescale and ±24 months for the interdecadal timescale. Results are not overly sensitive to the maximum lag size (Figure S14 in the supporting information).
3. The linear regression coefficient (at zero time lag) between local SAT and GMT ("a" in equation (1)) was greater than 1, indicating that local SAT had larger-magnitude variability than GMT.

$$\mathrm{SAT} = a \times \mathrm{GMT} + b \tag{1}$$

This condition ensured that ROSIs would be regions where local SAT variability worked to *enhance* the magnitude of GMT variability. A regression coefficient less than 1, even with a perfect correlation, would imply that local SAT variability worked to reduce the magnitude of GMT variability. However, results are not overly sensitive to the inclusion/exclusion of this criterion in the ROSI definition (Figure S14).

The goal of imposing these constraints was to identify the locations over the globe that were most responsible for GMT variability while disregarding those locations that primarily responded to global variability or tended to damp GMT variability.

It should be noted that other definitions of ROSIs are possible and the present definition excludes certain variability that could justly be argued to be "influential" on GMT. For example, local modes of variability may lag GMT in time but still play a major role in *maintaining* a GMT anomaly. Additionally, even if a local mode leads GMT, it may lead by a longer amount of time than the maximum lag length imposed in our ROSI definition. For example, the North Atlantic Oscillation has been shown to lead Northern Hemisphere mean temperature by 15–20 years [*Li et al.,* 2013]. In this case the ROSI would not identify the "original cause" of the large-scale variability but rather a more proximate cause of the large-scale variability.

3. Unforced Variability in GCMS and in Observations

In order to identify the geographic locations that have the largest association with unforced GMT variability, it was necessary to isolate the unforced component of variability from both observations and GCMs. For GCMs, we utilized preindustrial control runs that incorporated no external radiative forcings, and thus, all variability was necessarily unforced. We used 34 of these runs (first 2400 months, deseasonalized) from the Coupled Model Intercomparison Project Phase 5 (CMIP5) multimodel ensemble [*Taylor et al.,* 2011] and removed any long-term model drift (via linear detrending at each global grid location) that may have been due to incomplete model spin-up.

For observations we used the monthly NASA Goddard Institute for Space Studies (GISS) Surface Temperature analysis [*Hansen et al.,* 2010] from 1880 to 2013 because it provided the most extensive spatial coverage of the three most widely used instrumental data sets (the others being HadCRUT4 and NOAA Merged Land-Ocean Surface Temperature Analysis). In order to obtain unforced variability from the observational record, it was necessary to remove the component of variability that resulted from external radiative forcings. This was done in two separate ways, referred to below as Method (1) and Method (2).

In Method (1), unforced variability was obtained by subtracting the CMIP5 "Historical" (1900–2005) and "RCP 6.0" (2006–2013) experiment ensemble mean (representing externally forced variability) from the observational data set at each point in space and time (see *Ting et al.* [2009] for a detailed explanation of this method). Only those GCMs that participated in both the Historical and RCP 6.0 experiments were incorporated in the ensemble mean to avoid any discontinuities that might arise from different GCMs participating in each experiment. Method (1) presumes that the CMIP5 ensemble mean accurately represents the temporal and spatial structure of forced variability over the contemporary climate record. However, some studies have implied that the time-varying aerosol forcing in the CMIP5 historical experiment (which has a high degree of uncertainty [*Hansen et al.,* 2011; *Otto et al.,* 2013; *Suzuki et al.,* 2013]) has been "overfit" to interdecadal variations in GMT over parts of the twentieth century [*Chylek et al.,* 2014; *DelSole et al.,* 2010; *Tung and Zhou*, 2013; *Wu et al.,* 2011], and thus, it masks some interdecadal unforced variability over that time ("overfitting" masks unforced variability by mistakenly attributing it to time-varying external forcings). To allow for this possibility, we also obtain unforced variability in the observational record via Method (2), in which time series were detrended with empirical mode decomposition [*Huang et al.,* 1998] at every grid point. This method is similar in concept to a linear detrend except that it allows for the slope of the secular component (representing forced change) to vary in time, and thus, it is better suited than linear detrending for isolating unforced variability [*Wu et al.,* 2011, 2007].

Once the unforced variability was obtained both in GCMs and in observations, variations were decomposed into subdecadal and interdecadal components. The interdecadal component was identified with a low-pass filter (Locally Weighted Scatterplot Smoothing [*Cleveland*, 1979]) that passed variability on the timescale of 120 months (10 years) and longer (results are not particularly sensitive to the use of different low-pass filters or different cutoff timescales, see supporting information). The subdecadal component was defined as the residual of a given time series after the interdecadal component was subtracted. Grid level SAT time series as well as GMT time series were both decomposed into subdecadal and interdecadal components prior to subsequent analysis.

4. GCM-by-GCM ROSIs

4.1. Subdecadal Timescale Variability

As stated above, a variety of methodologies have established that ENSO variability has an impact on GMT at subdecadal timescales [*Foster and Rahmstorf*, 2011; *Privalsky and Jensen*, 1995; *Trenberth et al.,* 2002; *Wigley*, 2000]. However, *Banholzer and Donner* [2014] recently suggested that central Pacific El Niño events (i.e., Dateline El Niño or El Niño Modoki events [*Ashok et al.,* 2007; *Trenberth and Stepaniak*, 2001]) may have a much weaker influence on GMT than traditional eastern Pacific El Niño events. This result illustrates that there is still much to learn about the specific causes of unforced GMT variability, even at the subdecadal timescale, and thus, it is useful to document the regions most associated with subdecadal GMT variability in CMIP5 GCMs.

In all 34 GCMs, as well as in both observational estimates using different techniques to isolate unforced variability, there is a positive relationship between tropical Pacific SAT and GMT at the subdecadal timescale

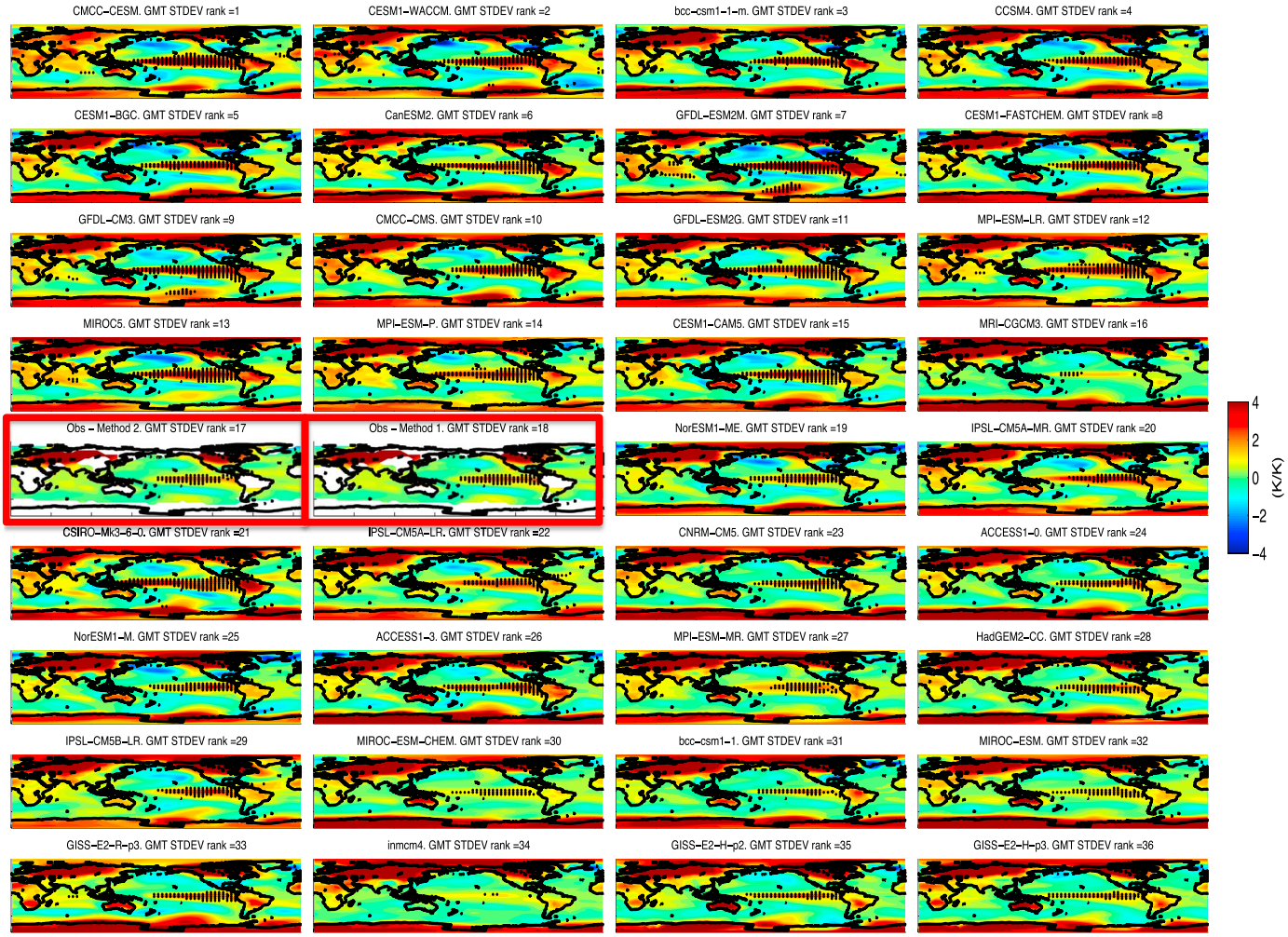

Figure 1. Local unforced SAT regressed against unforced GMT at the subdecadal timescale. ROSIs are represented with stippling. Panels are arranged from top left to bottom right by the standard deviation of their subdecadal GMT time series (rankings are displayed in the panel headings). The red-framed panels correspond to observations. For observations, only those locations with continuous time series available from 1880 to 2013 are colored.

(Figure 1) and tropical Pacific SAT tends to lead GMT in time (Figure S1). Additionally, in every GCM but two (MRI-CGCM3 and inmcm4), and in both observational estimates, the ROSI extended to the west coast of South America which supports the notion that traditional, eastern Pacific ENSO events have the largest impact on GMT [*Banholzer and Donner*, 2014]. Most GCMs also had relatively large regression coefficients (*a* in equation (1)) in the Polar Regions and in the tropical Atlantic and Indian Ocean. These regions, however, were characterized by SAT variability that tended to lag behind the GMT, and thus, they were not classified as ROSIs (Figure S1).

The standard deviations of the two observed subdecadal GMT time series were ranked seventeenth and eighteenth out of 36 (Figure 1), which suggests that there is not a systematic GMT magnitude bias in the multimodel ensemble (despite large biases from individual GCMs). Also, the fact that the two observational standard deviations were so similar (~0.124 K for both Method (1) and Method (2)) indicates that this result is relatively insensitive to the method used to isolate unforced variability.

4.2. Interdecadal Timescale Variability

The eastern equatorial Pacific has been identified as a primary influence on subdecadal timescale GMT in numerous other studies with independent methodologies. Thus, the agreement of the ROSI methodology with these previous findings (section 4.1) suggests that it may be useful for illuminating the locations most associated with unforced GMT variability on the interdecadal timescale as well.

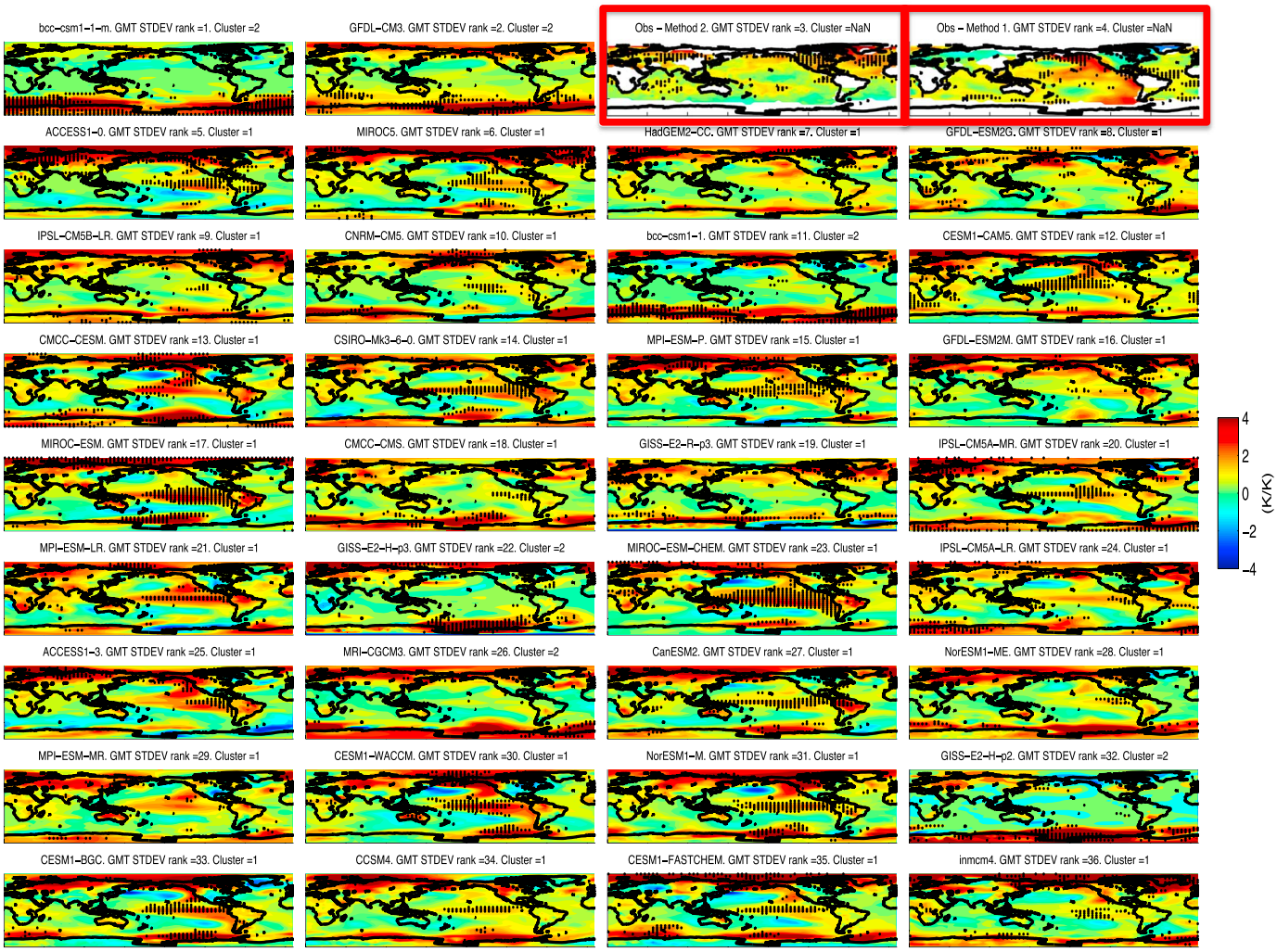

Figure 2. Same as Figure 1 but at the interdecadal timescale. Note that the panels are reordered by the standard deviation of their interdecadal component of GMT. The cluster assignment is discussed in section 5.1.

Figure 2 shows the regression coefficients between local SAT and GMT as well as the ROSIs at the interdecadal timescale (lead-lag times are shown in Figure S2). The GCMs display a much more diverse range of patterns for the interdecadal timescale than for the subdecadal timescale. Additionally, ROSIs tend to be more spatially heterogeneous and dispersed across the globe instead of being concentrated exclusively in a single region.

Despite the large diversity of patterns apparent in Figure 2, only a few GCMs highlight the North Atlantic as a large ROSI (MIROC5, inmcm4, and GISS-E2-R-p3), although many show positive regression coefficients there: ACCESS1-0, MIROC5, IPSL-CM5B-LR, CNRM-CM5, CSIRO-Mk3-6-0, GFDL-ESM2M, GISS-E2-R-p3, IPSL-CM5A-LR, inmcm4, HadGEM2-CC, GFDL-ESM2-G, CMCC-CMS, and IPSL-CM5A-MR. Many GCMs with large positive regression coefficients in the North Atlantic are not identified as ROSIs because they tend to lag, rather than lead GMT change (Figure S2).

It is interesting to note, however, that even if the North Atlantic is not identified as a ROSI, dynamics in this region may affect unforced GMT variability through global teleconnections. In particular, relative warmth of the North Atlantic has been suggested to intensify the Pacific Walker Circulation and induce a negative IPO pattern in the Pacific [*Chikamoto et al.,* 2012; *Hong et al.,* 2013; *Kucharski et al.,* 2011; *McGregor et al.,* 2014] which, in turn, is usually associated with unforced GMT cooling [*Huber and Knutti*, 2014; *Kosaka and Xie*, 2013; *Meehl et al.,* 2011, 2013; *Risbey et al.,* 2014; *Trenberth and Fasullo*, 2013].

Under this paradigm, we may expect to see negative regression coefficients between North Atlantic SAT and GMT because a relatively cool North Atlantic should induce a weaker Pacific Walker Circulation, warmer central/eastern Pacific SATs, and warmer GMT overall. Several GCMs produce patterns reminiscent of this description (bcc-csm1-1, CMCC-CESM, CanESM2, and NorESM1-MECESM1-BGC) but the majority do not.

Most GCMs do indicate a large ROSI over the equatorial Pacific Ocean (ACCESS1-0, MIROC5, CNRM-CM5, CESM1-CAM5, CMCC-CESM, CSIRO-Mk3-6-0, MPI-ESM-PGMT, MIROC-ESM, IPSL-CM5A-MR, MPI-ESM-LR, MIROC-ESM-CHEM, ACCESS1, CanESM2, NorESM1, CESM1-WACCM, NorESM1, CESM1-BGC, CCSM4, CESM1-FASTCHEM, and inmcm4) which supports the results of a number of recent studies [*Huber and Knutti*, 2014; *Kosaka and Xie*, 2013; *Meehl et al.,* 2011, 2013; *Risbey et al.,* 2014; *Trenberth and Fasullo*, 2013]. However, some GCMs have very few ROSIs in the Pacific (or North Atlantic) and instead have ROSIs scattered across the globe (HadGEM2-CC and GFDL-ESM2G) or concentrated over the Southern Ocean/Antarctica (bcc-csm1-1-m, GFDL-CM3, bcc-csm1-1, GISS-E2-H-p3, MRI-CGCM3, and GISS-E2-H-p2). The diversity of patterns across the GCMs indicates that the results obtained from any single-model study should be interpreted with caution.

Ideally, it would be possible to robustly assess GCM performance by comparing the regression patterns in Figure 2 to observations. Unfortunately, this task is challenging because the observational regression pattern and ROSI distribution are highly sensitive to the method used to isolate unforced variability at the interdecadal timescale (red-framed panels in Figure 2). When Method (1) is used, the Pacific's SAT field stands out as being particularly influential on unforced GMT; however, when Method (2) is used, the North Atlantic's SAT field appears to be more associated with GMT. The difference between the two methods is also quite apparent in the GMT time series (red-framed panels in Figure 3). Method (2) produces a large downward fluctuation from the early 1940s to the late 1970s and a subsequent upward fluctuation until the mid-2000s, consistent with the unforced oscillation identified in *Swanson et al.* [2009], *Tung and Zhou* [2013], and *Wu et al.* [2011]. Conversely, Method (1) produces very little interdecadal unforced variability throughout the middle of the twentieth century and then produces a large downward trend from the late 1990s to the present which corresponds to the recent GCM overestimation of global warming [*Fyfe et al.,* 2013]. The disagreement between the two methods exemplifies the uncertainty of whether this interdecadal SAT variability, particularly over the North Atlantic region, can be attributed to time-varying aerosol forcing [*Booth et al.,* 2012; *Mann et al.,* 2014] or to unforced variability [*Chylek et al.,* 2014; *Ting et al.,* 2009; *Tung and Zhou*, 2013; *Wu et al.,* 2011; *Zhang et al.,* 2013]. In particular, Method (1) attributes more twentieth century North Atlantic SAT variability to external aerosol forcings because of the region's proximity to strong aerosol emissions in the GCMs. However, it is possible that the aerosol forcing in some GCMs may be overfit to observations, and thus, Method (1) may mistake some unforced variability for forced variability [*Zhang et al.,* 2013]. This remains an unsettled issue, and the purpose of the present work is not to resolve it. Instead, we simply note that observational estimates of unforced interdecadal variability are highly sensitive to the method used to remove the forced component of variability. Additionally, the modeled regression patterns and ROSI distributions over the Southern Ocean and Antarctica are very difficult to compare to observations due to lack of data coverage until the latter part of the twentieth century. These factors combine to make it exceedingly difficult to assess the performance of the GCMs at this timescale. Furthermore, there is little difference between simulated interdecadal variability between GCMs that closely matched observed subdecadal variability and GCMs that did not (Figure S3) indicates that subdecadal timescale skill is a poor constraint on interdecadal timescale features.

Despite the differences in the *phasing* of the observed unforced interdecadal GMT variability between Method (1) and Method (2), Figure 3 indicates that the *magnitude* of unforced GMT variability is relatively consistent. The two observational GMT time series had similar standard deviations (0.09 K for Method (1) and 0.1 K for Method (2)) and were ranked third and fourth out of 36. This suggests that the simulated interdecadal GMT variability in the CMIP5 multimodel ensemble may be biased low on average (this finding is also supported by the spectral comparison shown in Figure S4). In particular, the low bias appears to be a due mostly to reduced interdecadal variability simulated over most of the world oceans relative to observations (Figure S6). It should be noted, however, that the recent downward fluctuation apparent in the Method (1) time series might be inflated if the increase in radiative forcings has been overestimated over the past decade [*Fyfe et al.,* 2013; *Schmidt et al.,* 2014].

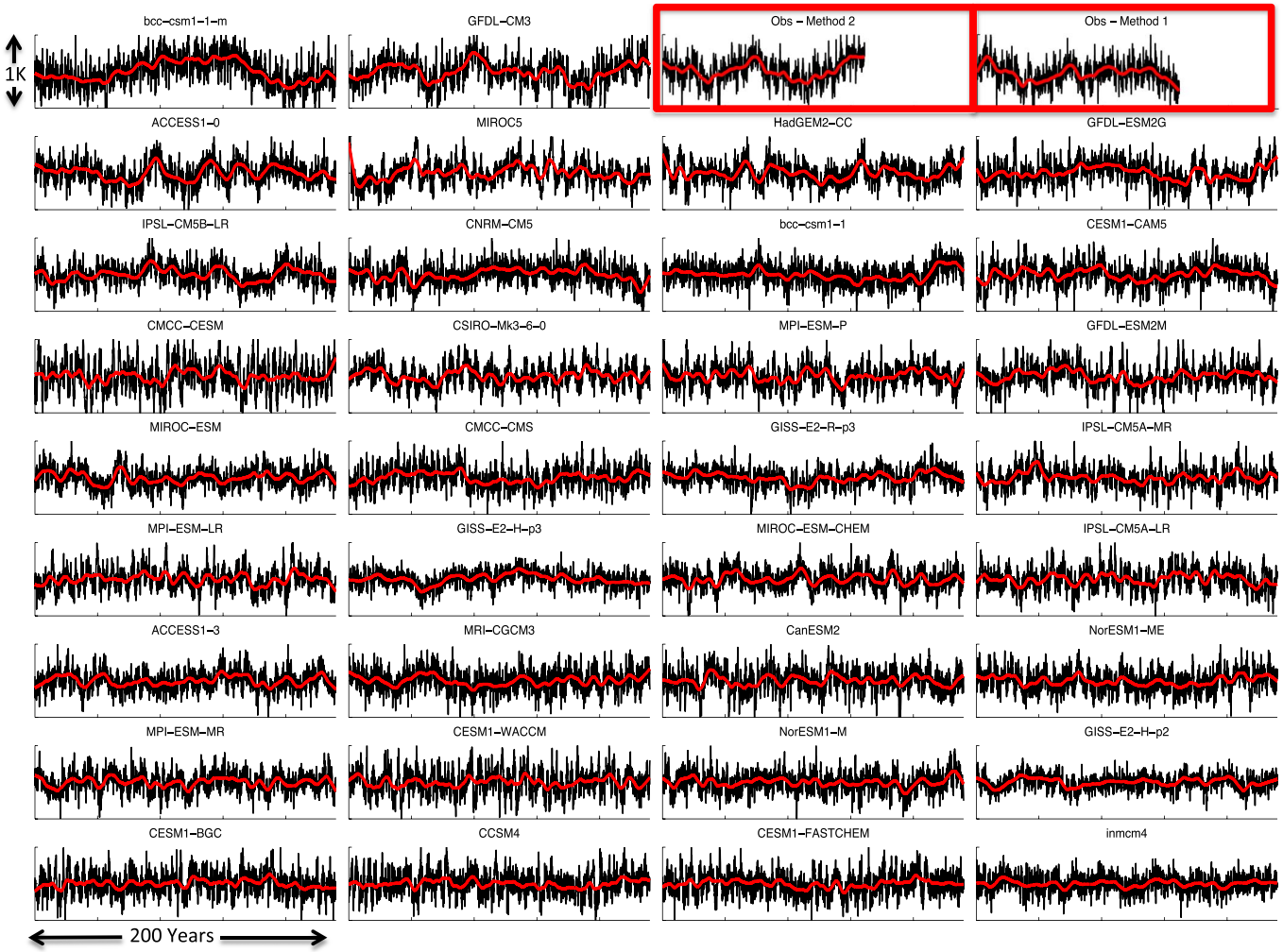

Figure 3. Unforced GMT time series for 34 GCMs (first 2400 months of unforced control run) as well as for observations from 1880 to 2013 (using two different methods to remove the forced component of variability). The red-framed panels correspond to observations. The interdecadal component of each time series is identified by the red line. Panels are arranged from top left to bottom right by the standard deviation of their interdecadal component. The ordinate ranges from −0.5 K to 0.5 K, while the abscissa range from year 1 to year 200 (1880–2079 for the observational panels).

5. Patterns Across the Multimodel Ensemble

5.1. Multimodel Mean Regression Patterns

Figure 4 shows the GCM mean regression relationship between local SAT and GMT at both the subdecadal and interdecadal timescales (Figures 4a–4c) as well as the cumulative spatial distribution of ROSIs (i.e., the number of GCMs that identified a given grid location as a ROSI) (Figures 4d–4f). For the interdecadal timescale, there was sufficient diversity among SAT versus GMT regression patterns (Figure 2) to support separating the GCMs into categories prior to averaging across models. Separating the GCMs into two categories with *k*-means clustering [*Mucha*, 1986] was useful in this regard as it divided the GCMs with a large Southern Ocean emphasis in their SAT versus GMT regression pattern from those with more of an emphasis on the Pacific Ocean (the cluster assignment for each GCM is shown in Figure 2). In order to gain insight on the underlying physical processes responsible for the simulated unforced GMT variability, GCM mean maps of anomalous sea level pressure (SLP, Figures 4g–4i), surface upward energy flux (Q_{sfc}, Figures 4j–4l), and top-of-atmosphere downward radiative flux (Q_{TOA}, Figures 4m–4o) regressed against GMT are also shown (a positive sign for either Q_{sfc} or Q_{TOA} indicates anomalous energy flux into the atmosphere). SLP is useful for assessing how large-scale atmospheric circulation and mass change with GMT, while Q_{sfc} and Q_{TOA} give insight into the geographic locations of anomalous energy flow into and out of the atmosphere

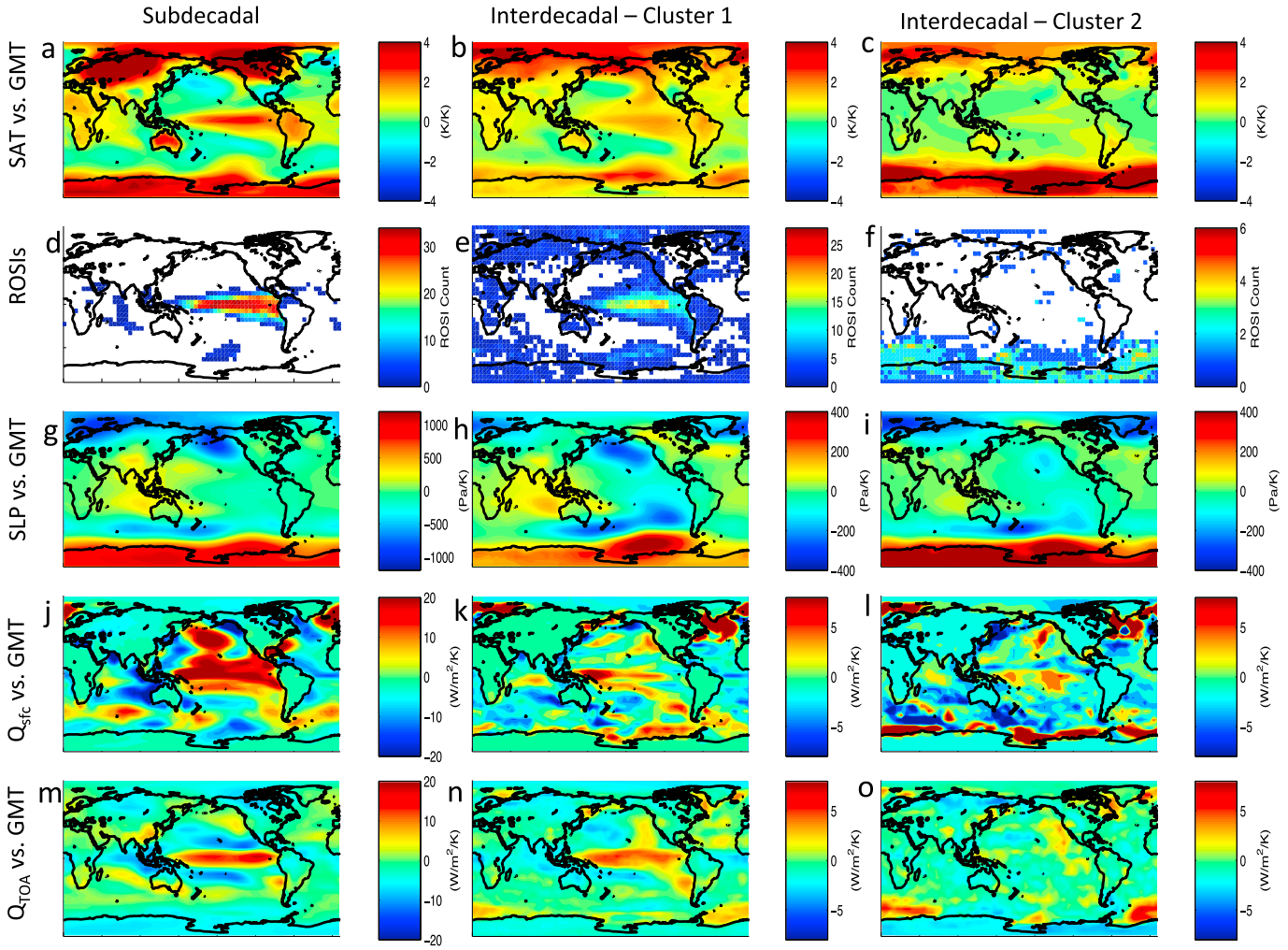

Figure 4. Local surface air temperature (SAT), sea level pressure (SLP), net upward surface energy flux (Q_{sfc}), and net downward top-of-atmosphere radiative flux (Q_{TOA}) regressed against GMT for each GCM and then averaged across GCMs for the (a, d, g, j, and m) subdecadal and interdecadal timescales ((b, e, h, k, and n) Cluster 1 and (c, f, i, l, and o) Cluster 2). The total number of ROSIs (summed across the GCMs) at each grid location is shown in the second row. The cluster assignment of each GCM at the interdecadal timescale is shown in Figure 2.

associated with GMT variation. In order to identify the most robust patterns, we focus here on the GCM mean results across the three categories (Subdecadal Timescale, Interdecadal Timescale Cluster 1, and Interdecadal Timescale Cluster 2).

5.1.1. Subdecadal Timescale

At the subdecadal timescale, the central equatorial Pacific represents a particularly influential location on GMT (Figures 4a and 4d). GMT tends to be anomalously high (low) when there is anomalously high (low) SLP over the western Pacific Ocean and Indian Ocean (Figure 4g). Such a SLP pattern is associated with weakened (strengthened) easterly equatorial trade winds and an anomalously warm (cool) eastern Pacific due partly to decreased (increased) upwelling from below the thermocline as well as the advection of anomalously warm (cool) surface water from the western (eastern) Pacific [*Neelin et al.,* 1998].

The relationship between Q_{sfc} in the equatorial Pacific and GMT indicates that a large portion of unforced variability in GMT can be traced to the anomalous sequestration (La Niña) and release (El Niño) of heat over the equatorial Pacific Ocean (Figure 4j). There is also a large positive Q_{sfc} anomaly in the north-central Pacific on subdecadal timescales which comes about because El Niño (La Niña) events are associated with enhanced (reduced) convection at the equator [*Trenberth et al.,* 1998] and a quasi-stationary Rossby wave response that causes a stronger (weaker) Aleutian Low. The change in the Aleutian Low strength implies

anomalous northerly (southerly) winds over the north-central Pacific and thus anomalously positive (negative) Q_{sfc} [*Alexander*, 1990; *Alexander et al.,* 2002; *Emery and Hamilton*, 1985; *Lau and Nath*, 1994; *Wang et al.,* 2012]. The opposite is the case along the west coast of North America, which gives rise to the "horseshoe-like" dipole pattern in North Pacific SAT (Figure 4a). Positive (negative) GMT anomalies are also associated with anomalously positive (negative) downward Q_{TOA} imbalances over the equatorial Pacific (Figure 4m). These imbalances are likely due to the ENSO shortwave heat flux feedback [*Bellenger et al.,* 2013; *Bony et al.,* 1997] in the eastern equatorial Pacific and changes in outgoing longwave radiation (due to changes in convection and atmospheric water vapor) in the western equatorial Pacific (Figure S7). These anomalous imbalances are partially offset by anomalies of the opposite sign over the subsident regions of the circulation in the subtropical Pacific in both hemispheres [*Pierrehumbert*, 1995].

5.1.2. Interdecadal Timescale

At the interdecadal timescale, Cluster 1's SAT regression pattern (Figure 4b) and ROSI distribution (Figure 4e) are suggestive of a large influence from low-frequency ENSO variability and/or the IPO on GMT. For Cluster 1, anomalously high (low) SLP over the western Pacific and Indian Ocean (Figure 4h) implies relaxed (enhanced) easterly trade winds which can cause the circulation of the Pacific shallow overturning cells to weaken (strengthen), leading to anomalously low (high) subsidence of warm water [*England et al.,* 2014; *Meehl et al.,* 2013] and anomalously high (low) Q_{sfc} over the western equatorial Pacific (Figure 4k). For Cluster 2, the SAT regression pattern (Figure 4c) and ROSI distribution (Figure 4f) are suggestive of a large influence from low-frequency variability over the Southern Ocean. The SLP anomalies over much of the midlatitudes are of the same sign but less intense than in Cluster 1 (Figure 4i), except over the Southern Ocean and Antarctica where the positive relationship between SLP (e.g., the Southern Annular Mode) and GMT is much stronger.

High (low) GMT in both interdecadal clusters is associated with anomalously high (low) Q_{sfc} over parts of the Southern Ocean (Figures 4k and 4i). For Cluster 1, this may be due to a teleconnection between the sea ice extent over the Pacific-facing Southern Ocean and interdecadal ENSO variability [*Okumura*, 2013; *Yuan*, 2004]. For Cluster 2, the large magnitude and spatial extent of the Q_{sfc} versus GMT regression pattern over the Southern Ocean suggest that dynamics involving variability in Antarctic Bottom Water formation and sea ice feedbacks may play a critical role in GMT variability in these GCMs [*Latif et al.,* 2013; *Martin et al.,* 2013].

Both Cluster 1 and Cluster 2 appear to receive at least some GMT variability from the Atlantic Ocean. In particular, when GMT is high (low), the North Atlantic Oscillation [*Hurrell*, 1995] tends to be positive (negative) (Figures 4h and 4i), and Q_{sfc} over the subpolar North Atlantic tends to be anomalously positive (negative), indicating a large anomalous flux of energy into (out of) the atmosphere (Figures 4k and 4i). This would suggest that high (low) GMT occurs during periods of high (low) oceanic heat convergence associated with corresponding changes in the Atlantic Meridional Overturning Circulation (AMOC) [*Gulev et al.,* 2013]. However, since there is not a significant ROSI count over the subpolar North Atlantic (Figures 4e and 4f), the AMOC influence on GMT in these GCMs may be nonlocal (i.e., the AMOCs influence may not be communicated through its effect on local SAT). This is consistent with the finding that variability in the AMOC is not independent from IPO variability in at least one GCM [*Meehl et al.,* 2013].

Anomalous Q_{TOA} flux also plays a role in interdecadal GMT variability for both clusters. Specifically, anomalously high (low) GMT is associated with anomalously positive (negative) Q_{TOA} flux over the central and eastern Pacific in Cluster 1 (Figure 4n). The eastern equatorial Pacific is characterized by large-scale atmospheric subsidence, relatively cool surface temperatures (for the latitude) and marine stratiform clouds [*Klein and Hartmann*, 1993] that have a net cooling effect on the surface [*Hartmann et al.,* 1992]. Therefore, a decrease (increase) in these clouds due to SAT warming (cooling) and increased (decreased) convection should cause a positive (negative) Q_{TOA} anomaly [*Sun et al.,* 2003; *Wallace et al.,* 1989] which can enhance (suppress) the initial SAT anomaly (Figure S7). In the western Pacific, SAT warming (cooling) is associated with increased (decreased) deep convective towers and atmospheric water vapor that can reduce (increase) outgoing longwave radiation sufficiently to cause a positive (negative) Q_{TOA} anomaly (Figure S7). Anomalously high GMT is also associated with anomalously positive Q_{TOA} over the Weddell Sea in both clusters (more so in Cluster 2 (Figure 4o) than in Cluster 1 (Figure 4n)). This provides evidence that many GCMs may have positive feedbacks on their unforced GMT variability that involve sea ice [*Drijfhout et al.,* 2013; *Latif et al.,* 2013].

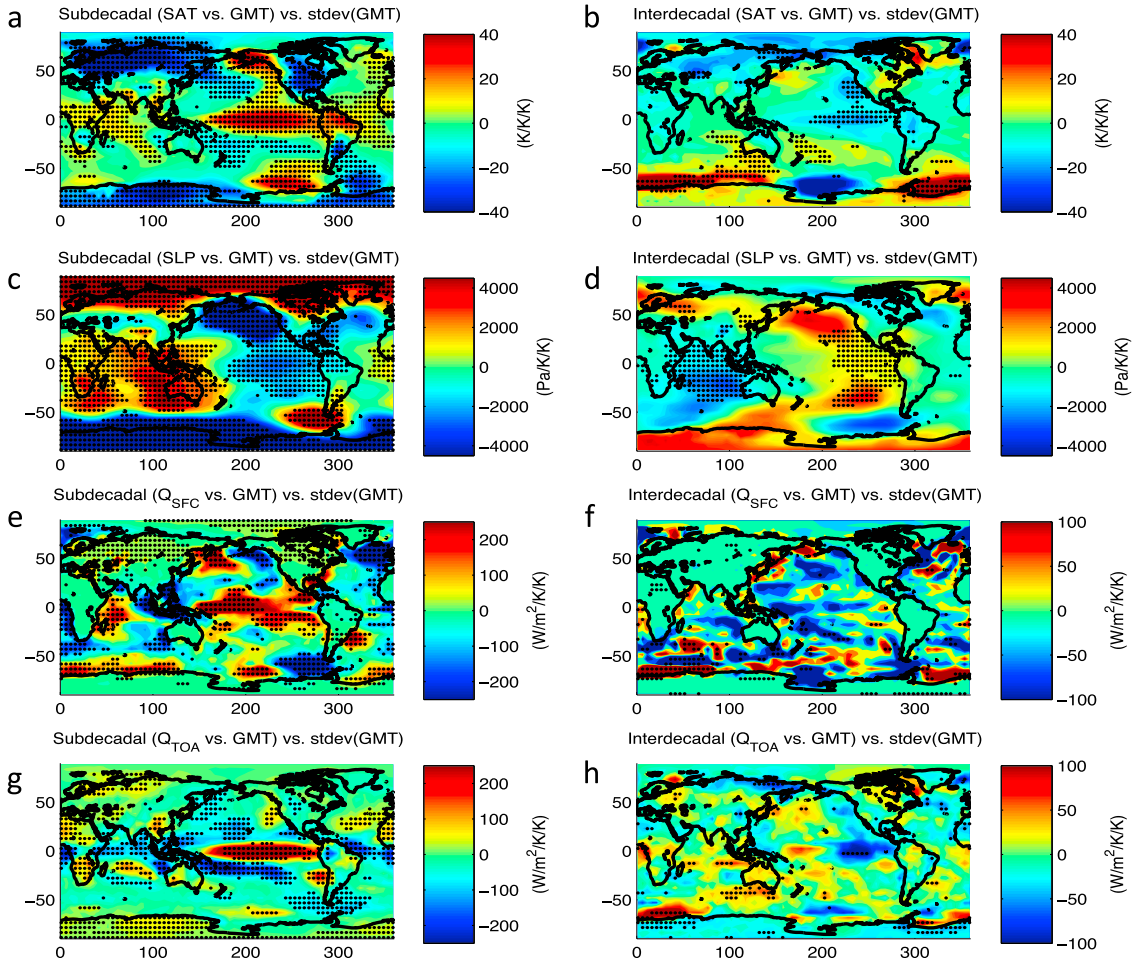

Figure 5. Intermodel regression of the regression coefficient of the listed variable versus GMT against the standard deviation of GMT at that timescale. Positive (negative) values indicate that GCMs with higher (lower) regression coefficients between the listed variable and that GCM's GMT tend to have a more (less) variable GMT at that timescale. Statistical significance of the intermodel linear regression is stippled.

5.2. Relationship Between the Magnitude of GMT Variability and Its Underlying SAT, SLP, Q_{sfc}, and Q_{TOA} Regression Patterns

Figures 1 and 2 are ordered in terms of the standard deviation of GMT at their respective timescales. From visual inspection, GCMs with more variable GMT tend to have different SAT versus GMT regression patterns than GCMs with less variable GMT. For example, at the subdecadal timescale (Figure 1), several of the GCMs with the most variable GMT (top left of Figure 1) have a higher positive SAT versus GMT regression coefficient over the tropical eastern Pacific and a more negative SAT versus GMT regression coefficient over the midlatitude western Pacific in both hemispheres. This leads to the supposition that the magnitude of a GCM's GMT variability may be related to its underlying SAT versus GMT regression pattern. In order to investigate this, we regressed the local SAT versus GMT pattern for each GCM against the corresponding standard deviation of each GCM's GMT. Regression coefficients were calculated across GCM space in a manner similar to an analysis performed by *Soden and Vecchi* [2011]. The intermodel regression slopes are mapped in Figure 5 along with analogous calculations applied to the regression coefficients of SLP versus GMT, Q_{sfc} versus GMT, and Q_{TOA} versus GMT.

The subdecadal (SAT versus GMT) versus STDEV(GMT) plot (Figure 5a) indicates that GCMs with more variable GMT tend to have a more emphasized ENSO-like pattern with larger SAT versus GMT regression coefficients in the tropical Pacific as well as over Alaska and the southeast Pacific. Additionally, GCMs with more variable subdecadal GMT tend to have smaller SAT versus GMT regression coefficients over much of North America,

Eurasia, and Antarctica. This indicates that there is less land and polar amplification of ENSO SAT response in GMCs with more variable GMT. On the other hand, at the interdecadal timescale, GCMs with more variable GMT tend to have a less emphasized ENSO/IPO SAT versus GMT regression pattern (Figure 5b). Instead, GCMs with more variable GMT have a much stronger SAT versus GMT regression slope over the Weddell Sea and the Indian and Atlantic sectors of the Southern Ocean.

The subdecadal (SLP versus GMT) versus STDEV(GMT) pattern also indicates that ENSO-like variability is emphasized more in GCMs with large GMT variance. In particular, SLP tends to decrease more in the eastern Pacific and increase more over the Indian Ocean per degree of GMT warming (Figure 5c) for GCMs with more variable GMT. On the other hand, the opposite pattern is found at the interdecadal timescale where GCMs with more variable GMT tend to have a less-positive regression coefficient between SLP and GMT over the Indian Ocean and a less-negative regression coefficient over the eastern Pacific (Figure 5d).

At the subdecadal timescale, the (Q_{sfc} versus GMT) versus STDEV(GMT) plot (Figure 5e) indicates that larger anomalous heat fluxes over the tropical Pacific and northwest Pacific (per degree of GMT change) are associated with more variable GMT. Additionally, the subdecadal (Q_{TOA} versus GMT) versus STDEV(GMT) (Figure 5g) looks similar to the Q_{TOA} versus GMT pattern (Figure 4m) which indicates that larger positive TOA feedbacks in the central equatorial Pacific are associated with more variable GMT.

At the interdecadal timescale, the (Q_{sfc} versus GMT) versus STDEV(GMT) and the (Q_{TOA} versus GMT) versus. STDEV(GMT) (Figures 5f and 5h) are relatively noisy, and there are only a few locations with statistically significant intermodel regressions. It is the case that more Q_{TOA} and Q_{sfc} flux (per degree of GMT change) over parts of the Southern Ocean near Antarctica is associated with more variable GMT. In particular, GCMs with more variable GMT tend to have larger changes in absorbed shortwave radiation in these regions (Figure S8), implicating positive feedbacks involving sea ice. This may imply that GCMs that simulate the type of variability described in *Latif et al.* [2013] and *Martin et al.* [2013] are more likely to produce large-magnitude interdecadal GMT variability. More variable GMT is also associated with less Q_{TOA} flux (per degree of GMT) over the tropical eastern Pacific, which further supports the notion that GCMs with more variable GMT tend to have less of an emphasis on the IPO and more of an emphasis on dynamics in the Southern Ocean.

6. Summary

We have performed a regression analysis between local SAT and GMT variability in both GCMs and observations in order to document the geographic locations that are most associated with unforced GMT variability at both the subdecadal and interdecadal timescales. We defined Regions of Significant Influence (ROSIs) on GMT which are locations that had statistically significant SAT versus GMT correlations, had SAT that led GMT in time, and had a SAT versus GMT regression coefficient greater than 1 meaning that local SAT variability tended to enhance rather than damp GMT variability.

This study confirms that almost all CMIP5 GCMs act in accordance with the established finding that subdecadal timescale GMT variability is associated with ENSO activity. In particular, GMT variability tends to be associated with equatorial Pacific SAT anomalies that extend to the west coast of South America supporting recent observationally based findings [*Banholzer and Donner*, 2014]. It was shown that the anomalous energy necessary to change subdecadal GMT comes primarily from the tropical and northern Pacific Ocean (with contributions from positive feedbacks at the top of the atmosphere in the equatorial Pacific). Additionally, the magnitude of GCM-simulated subdecadal variability was not systematically biased (i.e., there were roughly an equal number of GCMs that overestimated the magnitude as underestimated the magnitude compared to observations). At the subdecadal timescale, higher amplitude ENSO-like spatial patterns (per degree of GMT change) were shown to be associated with more variable GMT across the GCMs.

On the interdecadal timescale, the CMIP5 GCMs are relatively inconsistent in the spatial patterns that are most responsible for variability in GMT, and thus, any results from single-model studies should be interpreted with caution. Overall, most GCMs display a ROSI pattern that emphasizes the Pacific Ocean and is reminiscent of the Interdecadal Pacific Oscillation (IPO). The North Atlantic (i.e., AMO) does not stand out as being particularly influential on GMT in most GCMs. Interestingly, SAT over the Southern Ocean especially near the Weddell Sea does have a strong association with GMT variability in many GCMs. Interdecadal GMT variability tends to be enhanced due to anomalous heat flux at the ocean surface (over the western equatorial Pacific, the

Southern Ocean, and the subpolar North Atlantic) as well as at the top of the atmosphere (over the equatorial and eastern Pacific, over the Weddell Sea, and over Baffin Bay and the Greenland Sea).

For interdecadal variability, observational regression patterns between SAT and GMT as well as the ROSI distribution were very sensitive to the method used to remove the forced variability from the record, making it difficult to validate the GCMs. The magnitude of unforced interdecadal GMT variability in observations, however, was relatively insensitive to the method used to remove the forced variability. The magnitude of observed unforced GMT variability was larger than in 32 GCMs (out of 34), which indicates that the GCM ensemble may systematically underestimate unforced GMT variability at the interdecadal timescale. GCMs with more variable GMT tend to have less of an emphasis on their tropical Pacific SAT versus GMT pattern and more of an emphasis on their Southern Ocean SAT versus GMT pattern indicating that GCMs with more vigorous Southern Ocean variability may be better able to simulate the correct magnitude of GMT variability.

Acknowledgments

We would like to acknowledge the World Climate Research Programme's Working Group on Coupled Modelling, which is responsible for CMIP, and we thank the climate modeling groups for making their model's (listed in the panels in Figures 1–3) output available for analysis. The CMIP5 data used for this study can be downloaded at http://cmip-pcmdi.llnl.gov/cmip5/data_portal.html. We acknowledge NASA Goddard Institute for Space Studies Surface Temperature Analysis (GISTEMP) for making their data available for download at http://data.giss.nasa.gov/gistemp/. We would also like to acknowledge Heidi Winner for providing editorial services. This work was partially supported by NSF grant AGS-1147608.

References

Alexander, M. (1990), Simulation of the response of the North Pacific Ocean to the anomalous atmospheric circulation associated with El Niño, *Clim. Dyn.*, *5*(1), 53–65, doi:10.1007/BF00195853.

Alexander, M. A., I. Bladé, M. Newman, J. R. Lanzante, N.-C. Lau, and J. D. Scott (2002), The atmospheric bridge: The influence of ENSO teleconnections on air–sea interaction over the global oceans, *J. Clim.*, *15*(16), 2205–2231, doi:10.1175/1520-0442(2002)015<2205:TABTIO>2.0.CO;2.

Ashok, K., S. K. Behera, S. A. Rao, H. Weng, and T. Yamagata (2007), El Niño Modoki and its possible teleconnection, *J. Geophys. Res.*, *112*, C11007, doi:10.1029/2006JC003798.

Banholzer, S., and S. Donner (2014), The influence of different El Niño types on global average temperature, *Geophys. Res. Lett.*, *41*, 2093–2099, doi:10.1002/2014GL059520.

Bellenger, H., E. Guilyardi, J. Leloup, M. Lengaigne, and J. Vialard (2013), ENSO representation in climate models: From CMIP3 to CMIP5, *Clim. Dyn.*, *1–20*, doi:10.1007/s00382-013-1783-z.

Bindoff, N., et al. (2013), IPCC AR5, CH 10: Detection and attribution of climate change: From global to regional, *Rep*.

Bony, S., K. M. Lau, and Y. C. Sud (1997), Sea surface temperature and large-scale circulation influences on tropical greenhouse effect and cloud radiative forcing, *J. Clim.*, *10*(8), 2055–2077, doi:10.1175/1520-0442(1997)010<2055:SSTALS>2.0.CO;2.

Booth, B. B. B., N. J. Dunstone, P. R. Halloran, T. Andrews, and N. Bellouin (2012), Aerosols implicated as a prime driver of twentieth-century North Atlantic climate variability, *Nature*, *484*(7393), 228–232. [Available at http://www.nature.com/nature/journal/v484/n7393/abs/nature10946.html - supplementary-information.]

Brown, P. T., E. C. Cordero, and S. A. Mauget (2012), Reproduction of twentieth century intradecadal to multidecadal surface temperature variability in radiatively forced coupled climate models, *J. Geophys. Res.*, *117*, D11116, doi:10.1029/2011JD016864.

Brown, P. T., W. Li, L. Li, and Y. Ming (2014), Top-of-atmosphere radiative contribution to unforced decadal global temperature variability in climate models, *Geophys. Res. Lett.*, 5175–5183, doi:10.1002/2014GL060625.

Chen, X., and K.-K. Tung (2014), Varying planetary heat sink led to global-warming slowdown and acceleration, *Science*, *345*(6199), 897–903, doi:10.1126/science.1254937.

Chikamoto, Y., M. Kimoto, M. Watanabe, M. Ishii, and T. Mochizuki (2012), Relationship between the Pacific and Atlantic stepwise climate change during the 1990s, *Geophys. Res. Lett.*, *39*, L21710, doi:10.1029/2012GL053901.

Chylek, P., J. D. Klett, G. Lesins, M. K. Dubey, and N. Hengartner (2014), The Atlantic Multidecadal Oscillation as a dominant factor of oceanic influence on climate, *Geophys. Res. Lett.*, 1689–1697, doi:10.1002/2014GL059274.

Cleveland, W. S. (1979), Robust locally weighted regression and smoothing scatterplots, *J. Am. Stat. Assoc.*, *74*(368), 829–836, doi:10.1080/01621459.1979.10481038.

Crowley, T. J., S. P. Obrochta, and J. Liu (2014), Recent global temperature "plateau" in the context of a new proxy reconstruction, *Earth's Future*, *2*(5), 281–294, doi:10.1002/2013EF000216.

DelSole, T., M. K. Tippett, and J. Shukla (2010), A significant component of unforced multidecadal variability in the recent acceleration of global warming, *J. Clim.*, *24*(3), 909–926, doi:10.1175/2010JCLI3659.1.

Delworth, T. L., and T. R. Knutson (2000), Simulation of early 20th century global warming, *Science*, *287*(5461), 2246–2250, doi:10.1126/science.287.5461.2246.

Delworth, T. L., R. Zhang, and M. E. Mann (2007), Decadal to centennial variability of the Atlantic from observations and models, in *Ocean Circulation: Mechanisms and Impacts—Past and Future Changes of Meridional Overturning*, edited by A. Schmittner, J. C. H. Chiang, and S. R. Hemming, pp. 131–148, AGU, Washington, D. C., doi:10.1029/173GM10.

Deser, C., M. A. Alexander, S.-P. Xie, and A. S. Phillips (2010), Sea surface temperature variability: Patterns and mechanisms, *Annu. Rev. Mar. Sci.*, *2*(1), 115–143, doi:10.1146/annurev-marine-120408-151453.

Drijfhout, S., E. Gleeson, H. A. Dijkstra, and V. Livina (2013), Spontaneous abrupt climate change due to an atmospheric blocking–sea-ice–ocean feedback in an unforced climate model simulation, *Proc. Natl. Acad. Sci. U.S.A.*, doi:10.1073/pnas.1304912110.

Easterling, D. R., and M. F. Wehner (2009), Is the climate warming or cooling?, *Geophys. Res. Lett.*, *36*, L08706, doi:10.1029/2009GL037810.

Emery, W. J., and K. Hamilton (1985), Atmospheric forcing of interannual variability in the northeast Pacific Ocean: Connections with El Niño, *J. Geophys. Res.*, *90*(C1), 857–868, doi:10.1029/JC090iC01p00857.

Enfield, D. B., A. M. Mestas-Nuñez, and P. J. Trimble (2001), The Atlantic Multidecadal Oscillation and its relation to rainfall and river flows in the continental U.S., *Geophys. Res. Lett.*, *28*(10), 2077–2080, doi:10.1029/2000GL012745.

England, M. H., S. McGregor, P. Spence, G. A. Meehl, A. Timmermann, W. Cai, A. S. Gupta, M. J. McPhaden, A. Purich, and A. Santoso (2014), Recent intensification of wind-driven circulation in the Pacific and the ongoing warming hiatus, *Nat. Clim. Change*, doi:10.1038/nclimate2106. [Available at http://www.nature.com/nclimate/journal/vaop/ncurrent/abs/nclimate2106.html - supplementary-information.]

Foster, G., and S. Rahmstorf (2011), Global temperature evolution 1979–2010, *Environ. Res. Lett.*, *6*(4), 044022, doi:10.1088/1748-9326/6/4/044022.

Fyfe, J. C., N. P. Gillett, and F. W. Zwiers (2013), Overestimated global warming over the past 20 years, *Nat. Clim. Change*, *3*(9), 767–769, doi:10.1038/nclimate1972. [Available at http://www.nature.com/nclimate/journal/v3/n9/abs/nclimate1972.html - supplementary-information.]

Gulev, S. K., M. Latif, N. Keenlyside, W. Park, and K. P. Koltermann (2013), North Atlantic Ocean control on surface heat flux on multidecadal timescales, *Nature*, *499*(7459), 464–467, doi:10.1038/nature12268. [Available at http://www.nature.com/nature/journal/v499/n7459/abs/nature12268.html - supplementary-information.]

Hansen, J., et al. (2005), Earth's energy imbalance: Confirmation and implications, *Science*, *308*(5727), 1431–1435, doi:10.1126/science.1110252.

Hansen, J., R. Ruedy, M. Sato, and K. Lo (2010), Global surface temperature change, *Rev. Geophys.*, *48*, RG4004, doi:10.1029/2010RG000345.

Hansen, J., M. Sato, P. Kharecha, and K. von Schuckmann (2011), Earth's energy imbalance and implications, *Atmos. Chem. Phys. Discuss.*, *11*(9), 27,031–27,105, doi:10.5194/acpd-11-27031-2011.

Hartmann, D. L., M. E. Ockert-Bell, and M. L. Michelsen (1992), The effect of cloud type of Earth's energy balance: Global analysis, *J. Clim.*, *5*, doi:10.1175/1520-0442.

Hasselmann, K. (1976), Stochastic climate models. Part I. Theory, *Tellus*, *28*(6), 473–485, doi:10.1111/j.2153-3490.1976.tb00696.x.

Hawkins, E., and R. Sutton (2009), The potential to narrow uncertainty in regional climate predictions, *Bull. Am. Meteorol. Soc.*, *90*(8), 1095–1107, doi:10.1175/2009BAMS2607.1.

Hong, S., I.-S. Kang, I. Choi, and Y.-G. Ham (2013), Climate responses in the tropical Pacific associated with Atlantic warming in recent decades, *Asia-Pacific J. Atmos. Sci.*, *49*(2), 209–217, doi:10.1007/s13143-013-0022-1.

Huang, N. E., Z. Shen, S. R. Long, M. C. Wu, H. H. Shih, Q. Zheng, N.-C. Yen, C. C. Tung, and H. H. Liu (1998), The empirical mode decomposition and the Hilbert spectrum for nonlinear and non-stationary time series analysis, *Proc. R. Soc. London, Ser. A*, *454*(1971), 903–995, doi:10.1098/rspa.1998.0193.

Huber, M., and R. Knutti (2014), Natural variability, radiative forcing and climate response in the recent hiatus reconciled, *Nature Geosci*, doi:10.1038/ngeo2228. [Available at http://www.nature.com/ngeo/journal/vaop/ncurrent/abs/ngeo2228.html - supplementary-information.]

Hunt, B. G. (2011), The role of natural climatic variation in perturbing the observed global mean temperature trend, *Clim. Dyn.*, *36*(3–4), 509–521, doi:10.1007/s00382-010-0799-x.

Hurrell, J. W. (1995), Decadal trends in the North Atlantic Oscillation: Regional temperatures and precipitation, *Science*, *269*(5224), 676–679, doi:10.1126/science.269.5224.676.

Keenlyside, N. S., M. Latif, J. Jungclaus, L. Kornblueh, and E. Roeckner (2008), Advancing decadal-scale climate prediction in the North Atlantic sector, *Nature*, *453*(7191), 84–88. [Available at http://www.nature.com/nature/journal/v453/n7191/suppinfo/nature06921_S1.html.]

Kerr, R. A. (2000), A North Atlantic climate pacemaker for the centuries, *Science*, *288*(5473), 1984–1985, doi:10.1126/science.288.5473.1984.

Klein, S. A., and D. L. Hartmann (1993), The seasonal cycle of low stratiform clouds, *J. Clim.*, *6*, doi:10.1175/1520-0442(1993)006<1587:TSCOLS>2.0.CO;2.

Kosaka, Y., and S.-P. Xie (2013), Recent global-warming hiatus tied to equatorial Pacific surface cooling, *Nature*, *501*(7467), 403–407, doi:10.1038/nature12534.

Kravtsov, S., and C. Spannagle (2008), Multidecadal climate variability in observed and modeled surface temperatures, *J. Clim.*, *21*(5), 1104–1121, doi:10.1175/2007JCLI1874.1.

Kucharski, F., I. S. Kang, R. Farneti, and L. Feudale (2011), Tropical Pacific response to 20th century Atlantic warming, *Geophys. Res. Lett.*, *38*, L03702, doi:10.1029/2010GL046248.

Latif, M., T. Martin, and W. Park (2013), Southern ocean sector centennial climate variability and recent decadal trends, *J. Clim.*, *26*(19), 7767–7782, doi:10.1175/JCLI-D-12-00281.1.

Lau, N.-C., and M. J. Nath (1994), A modeling study of the relative roles of tropical and extratropical SST anomalies in the variability of the global atmosphere-ocean system, *J. Clim.*, *7*(8), 1184–1207, doi:10.1175/1520-0442(1994)007<1184:AMSOTR>2.0.CO;2.

Leith, C. E. (1978), Predictability of climate, *Nature*, *276*(5686), 352–355.

Li, J., C. Sun, and F.-F. Jin (2013), NAO implicated as a predictor of Northern Hemisphere mean temperature multidecadal variability, *Geophys. Res. Lett.*, *40*, 5497–5502, doi:10.1002/2013GL057877.

Mann, M. E., B. A. Steinman, and S. K. Miller (2014), On forced temperature changes, internal variability and the AMO, *Geophys. Res. Lett.*, 3211–3219, doi:10.1002/2014GL059233.

Mantua, N. J., S. R. Hare, Y. Zhang, J. M. Wallace, and R. C. Francis (1997), A Pacific interdecadal climate oscillation with impacts on salmon production, *Bull. Am. Meteorol. Soc.*, *78*(6), 1069–1079, doi:10.1175/1520-0477(1997)078<1069:APICOW>2.0.CO;2.

Martin, T., W. Park, and M. Latif (2013), Multi-centennial variability controlled by Southern Ocean convection in the Kiel Climate Model, *Clim. Dyn.*, *40*(7–8), 2005–2022, doi:10.1007/s00382-012-1586-7.

McGregor, S., A. Timmermann, M. F. Stuecker, M. H. England, M. Merrifield, F.-F. Jin, and Y. Chikamoto (2014), Recent Walker circulation strengthening and Pacific cooling amplified by Atlantic warming, *Nat. Clim. Change*, doi:10.1038/nclimate2330. [Available at http://www.nature.com/nclimate/journal/vaop/ncurrent/abs/nclimate2330.html - supplementary-information.]

Meehl, G. A., and H. Teng (2014), CMIP5 multi-model hindcasts for the mid-1970s shift and early 2000s hiatus and predictions for 2016–2035, *Geophys. Res. Lett.*, *41*, 1711–1716, doi:10.1002/2014GL059256.

Meehl, G. A., et al. (2009), Decadal prediction, *Bull. Am. Meteorol. Soc.*, *90*(10), 1467–1485, doi:10.1175/2009BAMS2778.1.

Meehl, G. A., J. M. Arblaster, J. T. Fasullo, A. Hu, and K. E. Trenberth (2011), Model-based evidence of deep-ocean heat uptake during surface-temperature hiatus periods, *Nat. Clim. Change*, *1*(7), 360–364. [Available at http://www.nature.com/nclimate/journal/v1/n7/abs/nclimate1229.html - supplementary-information.]

Meehl, G. A., A. Hu, J. M. Arblaster, J. Fasullo, and K. E. Trenberth (2013), Externally forced and internally generated decadal climate variability associated with the interdecadal Pacific oscillation, *J. Clim.*, *26*(18), 7298–7310, doi:10.1175/JCLI-D-12-00548.1.

Messié, M., and F. Chavez (2011), Global modes of sea surface temperature variability in relation to regional climate indices, *J. Clim.*, *24*(16), 4314–4331, doi:10.1175/2011JCLI3941.1.

Mucha, H. J. (1986), Späth, H.: Cluster dissection and analysis: Theory, FORTRAN programs, examples. (Translator: Johannes Goldschmidt.) Ellis Horwood Ltd Wiley, Chichester 1985. 226 pp. £25, *Biom. J.*, *28*(2), 182–182, doi:10.1002/bimj.4710280207.

Muller, R. A., J. Curry, D. Groom, R. Jacobsen, S. Perlmutter, R. Rohde, A. Rosenfeld, C. Wickham, and J. Wurtele (2013), Decadal variations in the global atmospheric land temperatures, *J. Geophys. Res. Atmos.*, *118*, 5280–5286, doi:10.1002/jgrd.50458.

Neelin, J. D., D. S. Battisti, A. C. Hirst, F.-F. Jin, Y. Wakata, T. Yamagata, and S. E. Zebiak (1998), ENSO theory, *J. Geophys. Res.*, *103*(C7), 14,261–14,290, doi:10.1029/97JC03424.

Okumura, Y. M. (2013), Origins of tropical Pacific decadal variability: Role of stochastic atmospheric forcing from the south Pacific, *J. Clim.*, *26*(24), 9791–9796, doi:10.1175/JCLI-D-13-00448.1.

Otto, A., et al. (2013), Energy budget constraints on climate response, *Nat. Geosci.*, *6*(6), 415–416, doi:10.1038/ngeo1836. [Available at http://www.nature.com/ngeo/journal/v6/n6/abs/ngeo1836.html - supplementary-information.]

Palmer, M. D., and D. J. McNeall (2014), Internal variability of Earth's energy budget simulated by CMIP5 climate models, *Environ. Res. Lett.*, *9*(3), 034016, doi:10.1088/1748-9326/9/3/034016.
Pierrehumbert, R. T. (1995), Thermostats, radiator fins, and the local runaway greenhouse, *J. Atmos. Sci.*, *52*(10), 1784–1806, doi:10.1175/1520-0469(1995)052<1784:TRFATL>2.0.CO;2.
Power, S., T. Casey, C. Folland, A. Colman, and V. Mehta (1999), Inter-decadal modulation of the impact of ENSO on Australia, *Clim. Dyn.*, *15*(5), 319–324, doi:10.1007/s003820050284.
Privalsky, V. E., and D. T. Jensen (1995), Assessment of the influence of ENSO on annual global air temperatures, *Dyn. Atmos. Oceans*, *22*(3), 161–178, doi:10.1016/0377-0265(94)00400-Q.
Risbey, J. S., S. Lewandowsky, C. Langlais, D. P. Monselesan, T. J. O'Kane, and N. Oreskes (2014), Well-estimated global surface warming in climate projections selected for ENSO phase, *Nat. Clim. Change*, doi:10.1038/nclimate2310.
Schlesinger, M. E., and N. Ramankutty (1994), An oscillation in the global climate system of period 65–70 years, *Nature*, *367*(6465), 723–726.
Schmidt, G. A., D. T. Shindell, and K. Tsigaridis (2014), Reconciling warming trends, *Nat. Geosci.*, *7*(3), 158–160, doi:10.1038/ngeo2105.
Semenov, V. A., M. Latif, D. Dommenget, N. S. Keenlyside, A. Strehz, T. Martin, and W. Park (2010), The impact of north Atlantic–Arctic multidecadal variability on northern Hemisphere surface air temperature, *J. Clim.*, *23*(21), 5668–5677, doi:10.1175/2010JCLI3347.1.
Smith, D. M., S. Cusack, A. W. Colman, C. K. Folland, G. R. Harris, and J. M. Murphy (2007), Improved surface temperature prediction for the coming decade from a global climate model, *Science*, *317*(5839), 796–799, doi:10.1126/science.1139540.
Soden, B. J., and G. A. Vecchi (2011), The vertical distribution of cloud feedback in coupled ocean-atmosphere models, *Geophys. Res. Lett.*, *38*, L12704, doi:10.1029/2011GL047632.
Stott, P. A., S. F. B. Tett, G. S. Jones, M. R. Allen, J. F. B. Mitchell, and G. J. Jenkins (2000), External control of 20th century temperature by natural and anthropogenic forcings, *Science*, *290*(5499), 2133–2137, doi:10.1126/science.290.5499.2133.
Stott, P. A., G. S. Jones, J. A. Lowe, P. Thorne, C. Durman, T. C. Johns, and J.-C. Thelen (2006), Transient climate simulations with the HadGEM1 climate model: Causes of past warming and future climate change, *J. Clim.*, *19*(12), 2763–2782, doi:10.1175/JCLI3731.1.
Sun, D., J. T. Fasullo, T. Zhang, and A. Roubicek (2003), On the radiative and dynamical feedbacks over the equatorial Pacific cold tongue, *J. Clim.*, *16*, doi:10.1175/2786.1.
Suzuki, K., J. C. Golaz, and G. L. Stephens (2013), Evaluating cloud tuning in a climate model with satellite observations, *Geophys. Res. Lett.*, *40*, 4464–4468, doi:10.1002/grl.50874.
Swanson, K. L., and A. A. Tsonis (2009), Has the climate recently shifted?, *Geophys. Res. Lett.*, *36*, L06711, doi:10.1029/2008GL037022.
Swanson, K. L., G. Sugihara, and A. A. Tsonis (2009), Long-term natural variability and 20th century climate change, *Proc. Natl. Acad. Sci. U.S.A.*, *106*(38), 16,120–16,123, doi:10.1073/pnas.0908699106.
Taylor, K. E., R. J. Stouffer, and G. A. Meehl (2011), An overview of CMIP5 and the experiment design, *Bull. Am. Meteorol. Soc.*, *93*(4), 485–498, doi:10.1175/BAMS-D-11-00094.1.
Ting, M., Y. Kushnir, R. Seager, and C. Li (2009), Forced and internal twentieth-century SST trends in the North Atlantic*, *J. Clim.*, *22*(6), 1469–1481, doi:10.1175/2008JCLI2561.1.
Trenberth, K. E., and J. T. Fasullo (2013), An apparent hiatus in global warming?, *Earth's Future*, doi:10.1002/2013EF000165.
Trenberth, K. E., and D. P. Stepaniak (2001), Indices of El Niño evolution, *J. Clim.*, *14*(8), 1697–1701, doi:10.1175/1520-0442(2001)014<1697:LIOENO>2.0.CO;2.
Trenberth, K. E., G. W. Branstator, D. Karoly, A. Kumar, N.-C. Lau, and C. Ropelewski (1998), Progress during TOGA in understanding and modeling global teleconnections associated with tropical sea surface temperatures, *J. Geophys. Res.*, *103*(C7), 14,291–14,324, doi:10.1029/97JC01444.
Trenberth, K. E., J. M. Caron, D. P. Stepaniak, and S. Worley (2002), Evolution of El Niño–Southern Oscillation and global atmospheric surface temperatures, *J. Geophys. Res.*, *107*(D8), AAC 5-1–AAC 5-17, doi:10.1029/2000JD000298.
Tung, K.-K., and J. Zhou (2013), Using data to attribute episodes of warming and cooling in instrumental records, *Proc. Natl. Acad. Sci. U.S.A.*, *110*(6), 2058–2063, doi:10.1073/pnas.1212471110.
Vimont, D. J. (2005), The contribution of the interannual ENSO cycle to the spatial pattern of decadal ENSO-like variability*, *J. Clim.*, *18*(12), 2080–2092, doi:10.1175/JCLI3365.1.
Wallace, J. M., T. P. Mitchell, and C. Deser (1989), The influence of sea-surface temperature on surface wind in the eastern equatorial Pacific: Seasonal and interannual variability, *J. Clim.*, *2*, doi:10.1175/1520-0442(1989)002<1492:TIOSST>2.0.CO;2.
Wang, H., A. Kumar, W. Wang, and Y. Xue (2012), Influence of ENSO on Pacific decadal variability: An analysis based on the NCEP climate forecast system, *J. Clim.*, *25*(18), 6136–6151, doi:10.1175/JCLI-D-11-00573.1.
Wigley, T. M. L. (2000), ENSO, volcanoes and record-breaking temperatures, *Geophys. Res. Lett.*, *27*(24), 4101–4104, doi:10.1029/2000GL012159.
Wilcox, L. J., E. J. Highwood, and N. J. Dunstone (2013), The influence of anthropogenic aerosol on multi-decadal variations of historical global climate, *Environ. Res. Lett.*, *8*(2), 024033, doi:10.1088/1748-9326/8/2/024033.
Wild, M. (2009), How well do IPCC-AR4/CMIP3 climate models simulate global dimming/brightening and twentieth-century daytime and nighttime warming?, *J. Geophys. Res.*, *114*, D00D11, doi:10.1029/2008JD011372.
Wu, Z., N. E. Huang, S. R. Long, and C.-K. Peng (2007), On the trend, detrending, and variability of nonlinear and nonstationary time series, *Proc. Natl. Acad. Sci. U.S.A.*, *104*(38), 14,889–14,894, doi:10.1073/pnas.0701020104.
Wu, Z., N. Huang, J. Wallace, B. Smoliak, and X. Chen (2011), On the time-varying trend in global-mean surface temperature, *Clim. Dyn.*, *37*(3–4), 759–773, doi:10.1007/s00382-011-1128-8.
Wyatt, M., and J. Curry (2013), Role for Eurasian Arctic shelf sea ice in a secularly varying hemispheric climate signal during the 20th century, *Clim. Dyn.*, 1–20, doi:10.1007/s00382-013-1950-2.
Yuan, X. (2004), ENSO-related impacts on Antarctic sea ice: A synthesis of phenomenon and mechanisms, *Antarct. Sci.*, *16*(4), 415–425, doi:10.1017/S0954102004002238.
Zhang, L., and C. Wang (2013), Multidecadal North Atlantic sea surface temperature and Atlantic meridional overturning circulation variability in CMIP5 historical simulations, *J. Geophys. Res. Oceans*, *118*, 5772–5791, doi:10.1002/jgrc.20390.
Zhang, R., T. L. Delworth, and I. M. Held (2007), Can the Atlantic Ocean drive the observed multidecadal variability in Northern Hemisphere mean temperature?, *Geophys. Res. Lett.*, *34*, L02709, doi:10.1029/2006GL028683.
Zhang, R., et al. (2013), Have aerosols caused the observed Atlantic multidecadal variability?, *J. Atmos. Sci.*, *70*(4), 1135–1144, doi:10.1175/JAS-D-12-0331.1.
Zhang, Y., J. M. Wallace, and D. S. Battisti (1997), ENSO-like interdecadal variability: 1900–93, *J. Clim.*, *10*(5), 1004–1020, doi:10.1175/1520-0442(1997)010<1004:ELIV>2.0.CO;2.
Zhou, J., and K.-K. Tung (2012), Deducing multidecadal anthropogenic global warming trends using multiple regression analysis, *J. Atmos. Sci.*, *70*(1), 3–8, doi:10.1175/JAS-D-12-0208.1.